ELSEVIER

Applied Surface Science 173 (2001) 327–338

applied surface science

www.elsevier.nl/locate/apsusc

Surface oxidation of Al–Cr–Fe alloys characterized by X-ray photoelectron spectroscopy

V. Demange[a], J.W. Anderegg[b], J. Ghanbaja[c], F. Machizaud[a], D.J. Sordelet[b,d], M. Besser[b], P.A. Thiel[b,e,*], J.M. Dubois[a]

[a]*Laboratoire de Science et Génie des Matériaux Métalliques (INPL-CNRS UMR 7584), Ecole des Mines, Parc de Saurupt, 54042 Nancy Cedex, France*

[b]*Ames Laboratory, Iowa State University, Ames, IA 50011, USA*

[c]*Service Commun de Microscopie Electronique à Transmission, UHP-Nancy 1, F-54042 Vandoeuvre-les-Nancy Cedex, France*

[d]*Department of Materials Science and Engineering, Iowa State University, Ames, IA 50011, USA*

[e]*Department of Chemistry, Iowa State University, Ames, IA 50011, USA*

Received 9 October 2000; accepted 21 December 2000

Abstract

We present X-ray photoelectron spectroscopy (XPS) measurements of several Al–Cr–Fe samples which are mixtures of approximants of the decagonal phase. Some samples also contain a hexagonal γ-brass phase. Our purpose is to evaluate the effect of chemical composition, particularly Cr content, on the response of the surface to oxidation. Under mild conditions only aluminium oxidizes, but under extreme conditions (water immersion at room temperature, or oxygen exposure at high temperatures), chromium oxidizes as well. XPS data also provide a measure of the oxide thickness. Cr has no discernible effect on oxide thickness when the oxidizing environment is the gas phase, but provides significant protection against water immersion, where high concentrations of Cr reduce the thickness by as much as 40%. These results for the Al–Cr–Fe samples are compared with results for approximants and quasicrystals in other systems. © 2001 Elsevier Science B.V. All rights reserved.

PACS: 61.44.Br; 81.65.Mq; 33.60.Fy; 68.35.Dv

Keywords: Approximants of decagonal phase; X-ray photoelectron spectroscopy; Transmission electron microscopy; Oxidation

1. Introduction

Quasicrystals and approximants possess very useful properties: low coefficients of friction, low adhesion, high hardness and good corrosion resistance [1–5]. Several XPS studies on such alloys have been presented already, particularly for Al–Cu–Fe, Al–Pd–Mn and Al–Cu–Fe–Cr samples [6–13]. These have shown that the oxidation-resistance of these Al-rich alloys is primarily due to the formation of a passivating skin of pure, or nearly pure, aluminium oxide. While the oxidation resistance is good, it is of interest to see whether it can be improved even further, for instance by the addition of Cr. This metal is known to enhance the oxidation-resistance of other metallic alloys, notably stainless steels and nickel-based systems

* Corresponding author. Tel.: +1-515-294-7871; fax: +1-515-294-4709.
E-mail address: thiel@ameslab.gov (P.A. Thiel).

0169-4332/01/$ – see front matter © 2001 Elsevier Science B.V. All rights reserved.
PII: S0169-4332(01)00011-3

[14]. We present here the results of an XPS study of a series of Al–Cr–Fe alloys. Our goal is to probe a variety of oxidizing environments, and in each to determine which metal oxidizes, to measure the oxide thickness, and to quantify variation in surface composition. We compare the behaviour of this class of alloys with that of quasicrystals and approximants having different compositions, studied by the authors cited above. This approach allows us to elucidate the role which Cr may play in oxidation in these alloys.

2. Experimental details

2.1. Sample characterization and preparation

We studied four alloys A–D in the Al–Cr–Fe ternary system. These alloys were prepared in Nancy by melting the pure metallic constituents in an induction furnace under a helium atmosphere. The resulting samples were annealed for 20 h, in a quartz device under a vacuum of about 5×10^{-5} Torr at temperatures in the range 900–1050°C, depending on the alloy. Each sample was analysed by transmission electron microscopy (TEM). Characteristics of each alloy are summarized in Table 1. Alloy A, with nominal composition $Al_{77.5}Cr_{16.5}Fe_6$, is a mixture of the orthorhombic O_1-Al–Cr–Fe and O-Al–Cr–Fe phases — approximants of the decagonal phase already observed in this ternary system [15–17] — and a hexagonal phase isostructural with the γ-brass phase γ_2-Al_8Cr_5 studied in [18]. We called this new phase γ_2-Al–Cr–Fe. We checked the isomorphism by X-ray diffraction. The coexistence of cubic and hexagonal phases with quasicrystals was already noticed in the systems Al–Cr–Cu [19–21], Al–Cr–Cu–Fe [22], and Ga–Fe–Cu–Si [23]. Dong [22] considered that the cubic γ-brass Al_4Cu_9 type of structure present in the Al–Cr–Cu–Fe system is an approximant of a quasicrystal. Alloy B has a nominal composition $Al_{72.5}Cr_{19.5}Fe_8$ and is a mixture of O_1-Al–Cr–Fe, γ_2-Al–Cr–Fe, and O_2-Al–Cr–Fe, first observed in this system but already present in Al–Cu–Cr–Fe system [24,25]. Alloy C, with nominal composition $Al_{72.5}Cr_{21.5}Fe_6$, is a mixture of the O_1-Al–Cr–Fe and the approximant orthorhombic O-Al–Cr–Fe. The alloy D, with nominal composition $Al_{67.6}Cr_{23.7}Fe_{9.1}$, consists of the single γ_2-Al–Cr–Fe phase. Fig. 1a displays the [0 0 0 1] transmission electron diffraction pattern (TEDP) of the hexagonal γ_2-Al–Cr–Fe phase, while Fig. 1b and c display the [0 1 0] TEDP and the [1 0 0] TEDPs of the O_2-Al–Cr–Fe. We do not know the proportions of all these phases in each sample; indeed, microprobe analysis gives a single (average) composition and imaging gives no contrast. Thus, these phases are so intimately mixed that we cannot distinguish them from each other.

The sample surfaces studied by XPS were polished using SiC grinding paper up to 1200 grit, and then using diamond paste up to 0.5 μm. The specimens were then cleaned with ethanol prior to the XPS analysis.

Table 1
Description of the alloys studied (note that the O-Al–Cr–Fe phase is a non-Fibonacci approximant; see [16] and [17] for details)

Alloy	Nominal composition	Structure	Characteristics	*a* (Å)	*b* (Å)	*c* (Å)
A	$Al_{77}Cr_{16.5}Fe_6$	Orthorhombic O_1-AlCrFe	Approximant (3/2; 2/1) of decagonal phase	32.5	12.2	23.6
		Orthorhombic O-AlCrFe	Approximant (1/1; ?) of decagonal phase	12.3	12.4	30.7
		Hexagonal phase	Isostructural with γ_2-brass Al_8Cr_5	12.7	12.7	7.9
B	$Al_{72.5}Cr_{19.5}Fe_8$	Orthorhombic O-AlCrFe	Approximant (1/1; ?) of decagonal phase	12.3	12.4	30.7
		Orthorhombic O_2-AlCrFe	Approximant (2/1; 2/1) of decagonal phase	19.9	12.4	23.2
		Hexagonal phase	Isostructural with γ_2-brass Al_8Cr_5	12.7	12.7	7.9
C	$Al_{72.5}Cr_{21.5}Fe_6$	Orthorhombic O_1-AlCrFe	Approximant (3/2; 2/1) of decagonal phase	32.5	12.2	23.6
		Orthorhombic O-AlCrFe	Approximant (1/1; ?) of decagonal phase	12.3	12.4	30.7
D	$Al_{67.6}Cr_{23.3}Fe_{9.1}$	Hexagonal phase	Isostructural with γ_2-brass Al_8Cr_5	12.7	12.7	7.9

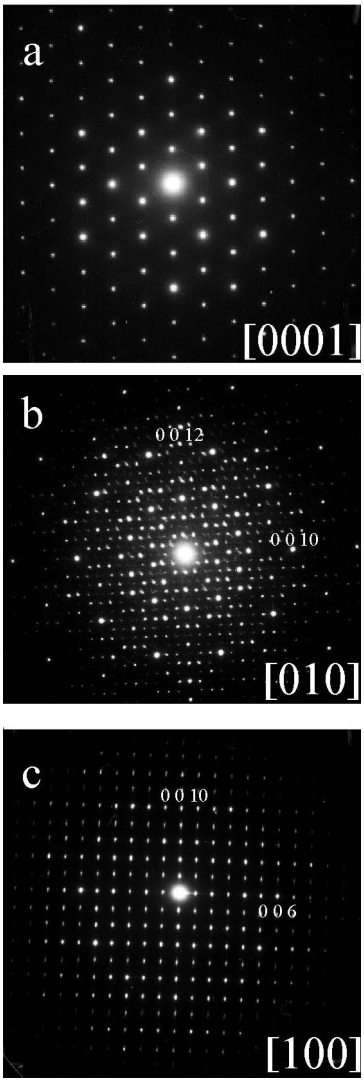

Fig. 1. TEDPs of (a) [0 0 0 1] hexagonal γ_2-Al–Cr–Fe phase, (b) [0 1 0] of the O_2-Al–Cr–Fe, and (c) [1 0 0] of the O_2-Al–Cr–Fe.

2.2. Oxidation conditions

The XPS instrument was a Physical Electronics 5500, fitted with an Omni Focus III lens system and controlled with PHI-Access software. The XPS energy scale was calibrated against Au $4f_{7/2}$ and Cu $2p_{3/2}$ peaks at 84.0 and 932.6 eV, respectively. The sample was mounted on a molybdenum block for XPS analysis, and placed in the XPS chamber. The temperature was measured with a Type K thermocouple. The base pressure of the chamber was about 3×10^{-10} Torr. The X-ray source provided monochromatized Al Kα radiation, and the take-off angle was fixed at $\theta = 45°$. The instrumental Gaussian full-width at half maximum (GFWHM), which characterizes the resolution, was 0.65 eV for the Al source.

The first step of the analysis consisted of cleaning the surface by sputtering with Ar^+ for 15–20 min, followed by annealing to 600°C to regenerate the surface. The oxygen that appeared at the surface after each cycle probably came from the bulk. It was necessary to remove this in order to have a meaningful measure of the effect of subsequent surface oxidation. Several cycles of sputtering–annealing were necessary to eliminate the oxygen on the surface, and the surface was considered clean when the oxygen signal was very weak. In the following, this sputter–anneal treatment preceded each oxidation experiment.

Next, each sample, A–D, was exposed to four oxidizing conditions. The first was oxygen gas leaked into the XPS chamber, via a directional doser, at room temperature. During exposure, the background pressure increased to about 3×10^{-8} Torr. Exposure was terminated when the aluminium oxide XPS peak stopped changing, i.e. when the surface was saturated in oxygen under these conditions. It occurred typically after 40 min. The second environment was also ultra high vacuum (UHV) with oxygen dosing, but with the sample at 450°C (the dosing time was typically 30 min). The third environment was air in a dessicator with $CaSO_4$. The exposure time was about 24 h and the relative humidity was about 6%. Finally, the fourth environment was pure liquid water in which the sample was immersed for about 15 h, so that the humidity was 100%. These oxidation conditions are summarized in Table 2. After each oxidation treatment, we recorded XPS peaks (shapes, positions and intensity) for the three elements of the alloy, for oxygen, and for the valence band. This entire procedure was repeated two times for each sample, in order to gauge the reproducibility of the results.

In addition, we studied the behaviour of pure aluminium under the same conditions of oxidation in order to compare it with aluminium in the alloys.

Another experiment was carried out in order to observe the reaction of the alloys under severe conditions of oxidation. We placed specimens of alloys A–D in a furnace under oxygen flow, first at 1040°C

Table 2
Description of oxidation conditions

1	Oxygen gas in XPS chamber	Room temperature	≅40 min
2	Oxygen gas in XPS chamber	450°C	≅30 min
3	Air (relative humidity 6%)	Room temperature	≅24 h
4	Pure liquid water	Room temperature	≅15 h

for 199 h, and next at 1080°C for 143 h. These two temperatures were chosen because both are close to the melting points of the alloys, which is about 1085°C for all the samples except sample D with a melting point of 1235°C. Since the four alloys were placed in the furnace together, we were limited by the melting temperature of the three lower-temperature alloys, A–C. These two time periods were chosen because oxidation, in terms of mass gain, seemed to be finished after 143 h at 1040°C and 119 h at 1080°C. For sample D, after 90 h at 1080°C, the curve decreased strongly (the difference in mass became negative), implying that sample D lost parts of its oxide layer.

3. Experimental results

3.1. Photoemission peak shapes and positions

We observe that alloys A–C respond similarly to oxidation. Consequently, we choose to show the results concerning, on one hand, only alloys A (Fig. 2) and D (Fig. 3) and, on the other hand, pure aluminium (Fig. 4), for comparison. In each figure, the photoemission spectra of the first row are obtained from clean and annealed samples as specified above. The following two rows represent samples after saturation with oxygen in UHV at room temperature and at 450°C, respectively. The next row shows the spectra after exposure to air for 24 h at room temperature. The last row presents the photoemission spectra of samples after immersion in water for 15 h.

The Al 2p line of the pure metal falls at 73 eV (the $2p_{1/2}$ and $2p_{3/2}$ contributions are unresolved) as does the Al 2p peak of the alloys. No shift can be seen in the position of this peak between pure aluminium and the alloys. The effects of the different oxidizing environments can be observed in the figures. As the degree of oxidation increases, a second peak appears at about 75 eV (Figs. 2 and 3b), and becomes increasingly important. This peak is the aluminium oxide line, expected at 73.7–74.1 eV for various forms of Al_2O_3 and at 74.2–74.3 eV for hydroxy-oxides [26].

The positions of the metallic Fe 2p peaks are given in the literature as 707 and 720 eV for the $2p_{3/2}$ and $2p_{1/2}$ contributions, respectively [27]. For Fe_2O_3, these peaks are given as 710.9 and 724.5 eV, respectively [27]. For all our samples, the metallic Fe 2p peaks are lower than the literature values by 0.5–0.7 eV. The relative intensity of the two peaks remains almost unchanged between the clean and oxidized samples after saturation with oxygen at 450°C. The last two figures show a smoothing of the shoulder due to plasmons at 724 eV. From panel i to panel j, a drastic change always takes place; the Fe 2p peaks disappear after water immersion.

The Cr 2p peaks in the pure metal (contributions $2p_{1/2}$ and $2p_{3/2}$) are reported at 574.4 eV and 583.6 eV [27]. In the oxide, they move up to 576.9 and 586.7 eV, respectively. For all our alloys, the metallic Cr peaks are lower than the literature values by 0.7–0.9 eV. Like iron, the relative intensity of the two Cr peaks remains almost unchanged for the first three environments. In Fig. 2n, there is a smoothing of the shoulder at 591 eV due to plasmon losses. In Fig. 2o, we see a drastic change in the photoemission spectra. In addition to the two peaks of metallic chromium, which remain slightly detectable, the two contributions expected for an oxide of Cr can be observed at higher binding energy.

For alloy D, the aluminium oxide peak is smaller than for the other three alloys, and the aluminium peak is slightly more visible. This reflects the fact that the aluminium oxide layer is thicker for alloys A–C than for alloy D, and so the oxide masks more and more the contribution of the bulk as the degree of oxidation increases. This is the subject of the next section. Also, for alloy D the intensity of the chromium oxide peaks in the case of water oxidation is higher than for the other alloys.

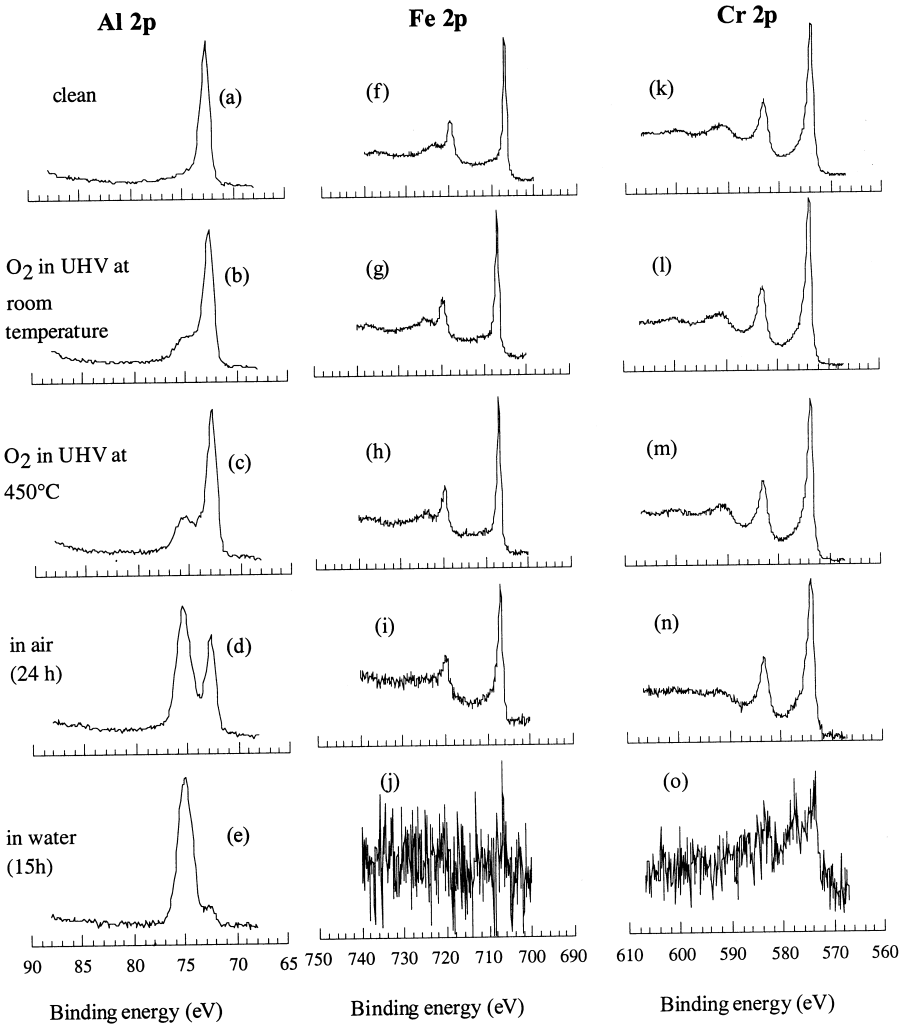

Fig. 2. Photoemission spectra of features characteristic of Al, Fe, and Cr in Alloy A, after various oxidation treatments as indicated.

3.2. Oxide thickness

Strohmeier [28] proposed a relation, which allows calculation of the oxide thickness on pure aluminium or on an aluminium alloy using the areas of photoemitted peaks. The assumption is made that the oxide layer is uniform. Actually, the oxide layer thickness obtained by this method is the total amount of all the types of oxides and hydroxy-oxides which are in the oxide layer. In addition, the oxide layer on metals is usually covered by a thin carbon contamination layer which can attenuate the photoemitted signals of oxide and bulk in an uncontrolled manner. Finally, in the case of water exposure, data show that aluminium is not the only metal to oxidize. Overall, the calculated values of oxide thickness are not rigoroursly exact, but give indications of trends. The Strohmeier formula is

$$d = \lambda_o \sin\theta \ell n\left(\frac{N_m}{N_o}\frac{\lambda_m}{\lambda_o}\frac{I_o}{I_m} + 1\right)$$

where d is the oxide layer thickness in Angstroms, θ the electron take-off angle, I_m and I_o are the intensities (or areas) of photoemitted peaks of metal and oxide, respectively, N_m and N_o the atomic densities of metallic atom in metal and in oxide, and λ_m and λ_o are the

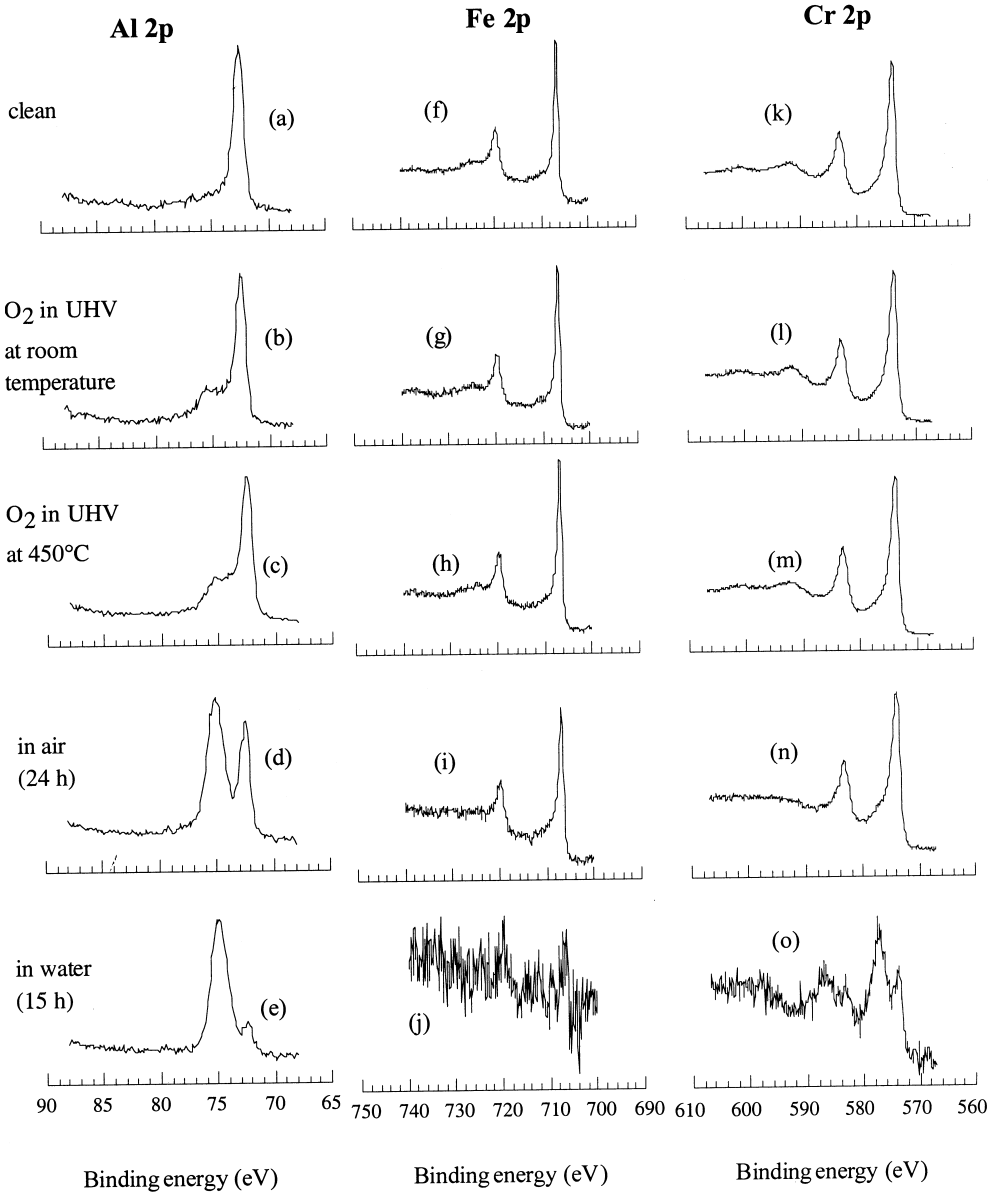

Fig. 3. Photoemission spectra of features characteristic of Al, Fe, and Cr in Alloy D, after various oxidation treatments as indicated.

inelastic free mean paths of the metallic and oxidic Al 2p photoelectrons. These last values have been given by Tanuma et al. [29] as 25.8 and 28.1 Å, respectively. The value N_o for the oxide is taken as 0.043 at./Å^3, the literature value for γ-Al_2O_3 [28]. The value N_m is calculated from the assumed atomic density of the alloys studied. The result, 0.068 at./Å^3, is close to the values of atomic densities of quasicrystals and their approximants and it was checked that a realistic uncertainty in this value introduces a negligible error in the calculations of oxide thickness. The results are compiled in Table 3.

As expected, the oxide thickness increases from low values for oxidation in vacuum at room temperature to higher values after water exposure. The thicknesses are close to each other for oxidation in vacuum. With

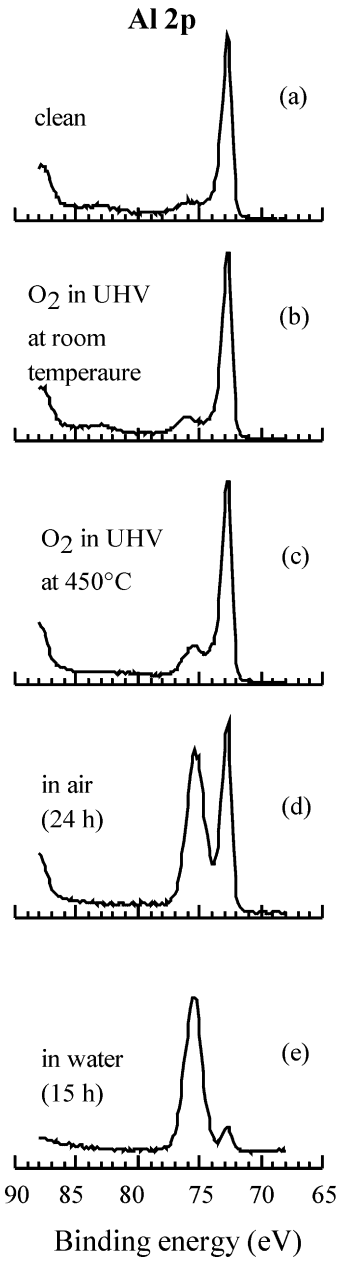

Fig. 4. Photoemission spectra of the Al 2p feature in pure Al, after various oxidation treatments as indicated.

air exposure, a difference appears between alloy A and the other alloys; the oxide layer for alloy A is slightly thicker. The differences become more pronounced after water exposure. The thickest oxide is observed for alloy A again, while the thinnest oxide corresponds to alloy D. The latter value of 49 Å is very small with respect to the severity of the oxidation condition. We note the fact that alloy D contains more chromium than the other three alloys.

Table 3
Aluminium oxide thickness

	Aluminium oxide thickness (Å)
Sample A	
After O_2 in vacuum	6±0.5
After O_2 in vacuum at 450°C	8.9
After air exposure	29
After water exposure	78±6
Sample B	
After O_2 in vacuum	6.5±0.1
After O_2 in vacuum at 450°C	8.2
After air exposure	22
After water exposure	61±4
Sample C	
After O_2 in vacuum	4.4±2
After O_2 in vacuum at 450°C	7.3
After air exposure	19
After water exposure	69±1
Sample D	
After O_2 in vacuum	4.1±3
After O_2 in vacuum at 450°C	7.6
After air exposure	23
After water exposure	49±2

3.3. Surface elemental composition

The PHI-Access software allows us to estimate the surface composition within the top 100 Å of the material, from the shape of XPS spectra. Table 4 presents percentages of each element, considering only the metals in the alloys (and ignoring any carbon or oxygen).

The surface composition for the clean samples is consistently enriched in iron relative to the nominal bulk composition given in Table 1, but the aluminium content is in good agreement with the expected value for this element. (Note that the XPS concentrations are extracted without specific calibration of sensitivity factors to this class of alloys, and so any agreement or disagreement between the bulk and surface values discussed until now may be fortuitous. The data are more reliable as indications of changes in concentration, as they are used in the following.) As oxidation

Table 4
Surface elemental composition

	Composition (%)		
	Al	Cr	Fe
Sample A			
Clean	74 ± 0.5	16 ± 0.8	10.35 ± 0.05
After O_2 in UHV	76.9	13.8	9.3
After O_2 in UHV at 450°C	79.8	11.8	8.4
After air exposure	87.3	9.2	3.5
After water exposure	94.6	4.8	0.6
Sample B			
Clean	72.35 ± 0.15	15.35 ± 0.15	12.05 ± 0.05
After O_2 in UHV	75.5 ± 0.5	13.8 ± 0.2	10.75 ± 0.75
After O_2 in UHV at 450°C	78.6	11.9	9.6
After air exposure	88	7.4	4.6
After water exposure	93.5 ± 0.1	6.4	0.1 ± 0.1
Sample C			
Clean	73.16 ± 0.84	16.43 ± 0.43	10.5 ± 0.5
After O_2 in UHV	78.4 ± 0.6	13.24 ± 0.26	8.4 ± 0.2
After O_2 in UHV at 450°C	78.9	12.1	9.9
After air exposure	87.4	7.6	5
After water exposure	92.5 ± 2.5	9.8 ± 5.2	0.75 ± 0.75
Sample D			
Clean	66.05 ± 1.05	19.9 ± 1.5	12
After O_2 in UHV	70.46 ± 2.46	19.6 ± 1.4	9.5 ± 1
After O_2 in UHV at 450°C	71.4	18.5	10.1
After air exposure	82.9	11.6	5.5
After water exposure	88 ± 2	10	1 ± 1

conditions progress, the surfaces become richer in aluminium, whereas they become depleted in chromium and iron. Notably, after water exposure, the iron content is almost 0. The alloy that becomes least enriched in aluminium at the surface is alloy D, which also exhibits the smallest oxide thickness (see Table 3). From this, we see also that the trend is the formation of an aluminium oxide layer at the surface.

3.4. High temperature oxidation

Fig. 5 shows the photoemission spectra for alloys A, B and D annealed at 1040°C in flowing O_2 at atmospheric pressure. This severe treatment leads to nearly complete transformation of surface aluminium into aluminium oxide, as shown by the Al XPS shape. The exception is alloy D, where the pure aluminium peak is more pronounced than in the other alloys. The iron spectrum of alloy A is very noisy and it is impossible to discern a peak. For alloy B, we can barely distinguish the Fe $2p_{3/2}$ line at about 707 eV. On the other hand, for alloy D, the iron peaks are clearly evident. Concerning the chromium spectra, the signal of alloy A is only noise. We can clearly see the chromium peaks in the spectrum of alloy B, and more clearly still in alloy D. We can also infer the presence of chromium oxide peaks in the broad region between 576 and 594 eV, particularly for alloy B.

In the same experiment at 1080°C, the first two samples present only the oxide peak in the aluminium spectra. The iron peaks are still visible. On the other hand, the chromium spectra are very noisy. For alloy D, the pure aluminium peak is detectable. The iron and chromium peaks are also visible, and we can discern evidence for chromium oxide in the chromium spectra. So, we can see here again that alloy D is less oxidized than the other two samples. The aluminium oxide thickness was calculated from the XPS spectra

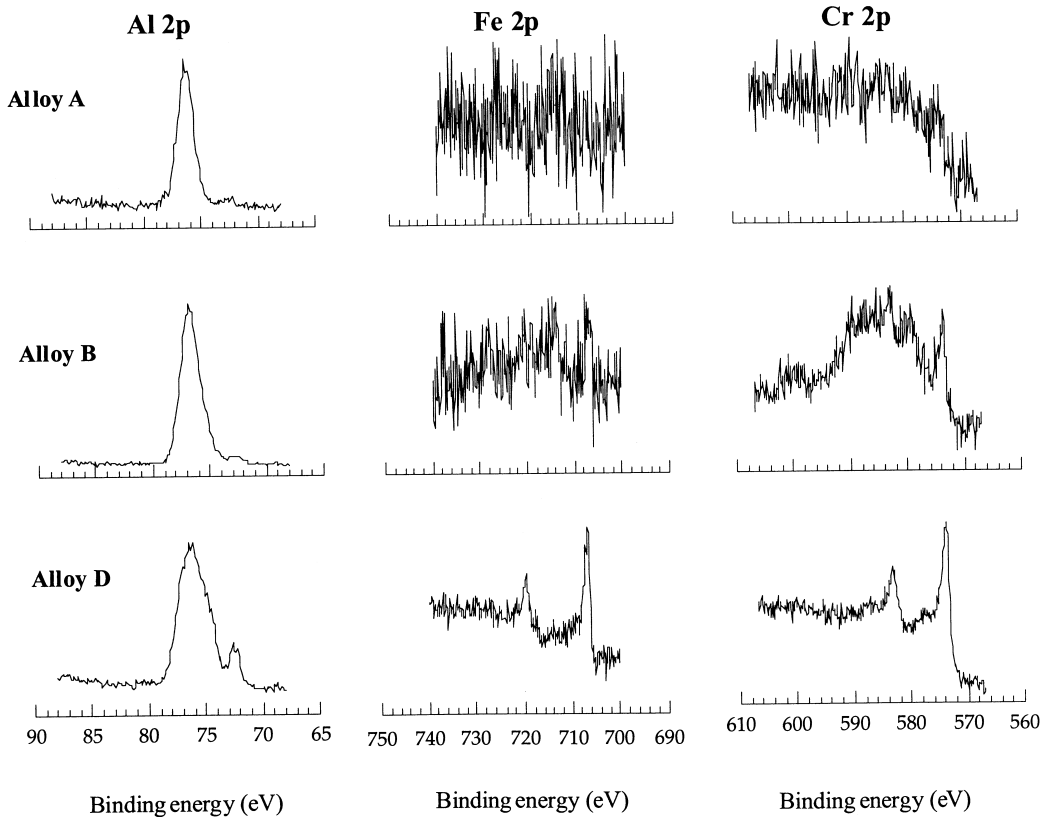

Fig. 5. Photoemission spectra for alloys A, B, and D annealed at 1040°C in flowing O_2 at atmospheric pressure for 119 h.

of aluminium. In the case of experiments at 1080°C, only alloy D presents an appropriate spectrum for such calculation. The results for both experiments are compiled in Table 5.

It appears, as expected, that the oxide of alloy D is thinner than those of the other alloys. In fact, it is very surprising that under such harsh conditions, these samples have such small oxide thicknesses and show such good oxidation resistance.

Table 5
Aluminium oxide thickness after oxidation at 1040°C for 119 h, and at 1080°C for 143 h, in flowing oxygen

	Oxide thickness (Å)		
	Alloy A	Alloy B	Alloy D
Experiment at 1040°C	69.5	61.6	54.5
Experiment at 1080°C	X	X	60.4

4. Discussion

It is useful to discuss the response of these materials in terms of the severity of the oxidizing environment. In most respects, immersion in water at room temperature seems to represent the harshest environment; this is the condition under which the Cr oxidizes most clearly and consistently (Figs. 2o, 3o and 5), under which the oxide layers are usually thickest (Tables 3 and 5), and under which the Al segregation is strongest (Table 4). Oxidation in flowing oxygen at 1040°C is competitive, at least in terms of oxide thickness. Oxidation in air at room temperature, in vacuum at 450°C, and in vacuum at room temperature, present progressively milder conditions.

The present study shows that, to zero order, the Al–Fe–Cr alloys behave very similarly to other Al-rich quasicrystals and approximants, specifically

Al–Cu–Fe, Al–Pd–Mn and Al–Cu–Fe–Cr alloys. In all cases, the surface composition becomes enriched in Al at the expense of the other elemental constituents upon oxidation; at the same time, Al is the only metal which oxidizes in vacuum, or in reasonably dry air at room temperature. Presumably, both observations stem from the preferential formation of an aluminium oxide, or aluminium hydroxy-oxide, overlayer.

With increasing severity of oxidizing environments, the Al enrichment becomes more pronounced, with a corresponding surface depletion in Cr and Fe for the Al–Cr–Fe alloys, and in Cu and Fe for the Al–Cu–Fe alloys. However, in the Cr-free Al–Cu–Fe alloys studied previously, the non-aluminium components remained protected from oxidation. This was true in spite of the fact that the pure elements Cu and Fe will oxidize in air, and pure Fe will oxidize even in vacuum [11–13]. Our samples display a different behaviour: while the Fe remains protected, the Cr is *not* inert against oxidation in liquid water or in flowing oxygen at high temperatures. This appears to be a fundamental difference in the Cr-containing alloys; the Cr *can* oxidize, under certain circumstances, in addition to the Al. A similar effect was already observed by Pinhero et al. [11] for Al–Cu–Fe–Cr (an orthorhombic approximant), where the presence of oxidized chromium was detected, particularly after water immersion.

Our experiments show that oxidation of Cr is associated with two other phenomena: formation of the deepest oxides (Table 3), and nearly complete depletion of Fe from the surface region probed by XPS (Table 4). The fact that only Al oxidizes in the thinnest oxides, but Cr oxidizes as well in the thicker oxides, suggests that the samples may respond in a sequential fashion to oxidation. We propose the following hypothesis. Oxidation of Al occurs first. Segregation of Al into the oxide leaves an Al-depleted layer underneath. If oxidation proceeds further, then oxidation of Cr becomes favourable in this interfacial region. A layer of chromium oxide forms preferentially beneath the aluminium oxide, driving the iron still deeper. Ultimately, the two oxides form a double barrier against further attack. Of course, it is too simplistic to envision two oxide layers separated by a sharp interface; a more realistic description is probably a gradated interface.

This hypothesis is consistent with the sequence of enthalpies of formation, for stoichiometrically equivalent oxides of the three metals. At room temperature, they are: -1675 kJ/mol for Al_2O_3, -1139.7 kJ/mol for Cr_2O_3, and -824.2 kJ/mol for Fe_2O_3 [30]. It is also consistent with the previous angle-resolved XPS data of Pinhero et al. [11], which indicated that the oxidized chromium in Al–Cu–Fe–Cr lies below the oxidized aluminium.

If this hypothesis is correct, then the oxide thicknesses reported in Tables 3 and 4 are subject to considerable error, *in those cases where Cr oxidizes*. The values extracted by the Strohmeier approach and reported in the tables would be intermediate between two limiting values: *smaller* than the thickness of the total $(Al + Cr)$ oxide layer, but *larger* than the thickness of the Al oxide component alone.

It is of interest to compare the depths of the oxides formed in our Al–Cr–Fe alloys with those reported for other aluminium-based quasicrystalline alloys and approximants. The response of our alloys is of the same order of magnitude as observed for the other systems. However, closer inspection reveals that our alloys do respond differently. After oxidation in air and in water, they are among the least-oxidized alloys. Particularly, alloy D presents a very low value of oxide depth after water immersion.

Could this behaviour — thinner oxides on the Al–Cr–Fe alloys — be due to a systematic error in measuring oxide thickness, because of the contribution of the Cr oxide? We think not, for two reasons. First, the trend is observed even after air oxidation at room temperature, where Cr does not oxidize measurably. Second, where Cr *does* oxidize, the thickness of the total $(Al + Cr)$ oxide could be considerably larger than reported here, but the value of the Al oxide component alone (if it is regarded as a distinct layer) could not. The comparison in Table 6 is being made to literature data for alloys which (with only one exception) form *only* Al oxides. Hence, the comparison should be regarded as that of a maximum value of an Al oxide on the Al–Cr–Fe alloys, against the less ambiguous values of the Al oxide on the other alloys.

Instead, we believe that the formation of thinner oxides on the Al–Cr–Fe alloys is mainly due to the Cr content, not to a systematic measurement error. The hypothesis described above then leads to a picture in

Table 6
Oxide thickness for different approximants or quasicrystalline alloys and for pure aluminium. Italic characters show results of the present study

Alloy	O_2 in vacuum (Å)
QC-AlPdMn[a]	8.5
Alloy B	*6.5±0.1*
Alloy A	*6±0.5*
β-AlCuFe[b]	5.1±1.5
QC-AlPdMn[c]	5
ψ-AlCuFe[b]	4.7±1
Al	*4.4*
C	*4.4±2*
λ-AlCuFe[b]	4.3±0.4
D	*4.1±3*
Al[c]	4
	In air (Å)
Al[c]	30
QC-AlPdMn[c]	29
A	*29*
β-AlCuFe	27
AlCuFeCr[b]	27±1.4
β-AlCuFe[b]	26±0.3
QC-AlPdMn[a]	26
O_1-AlCuFeCr	25
λ-AlCuFe[b]	24±2.3
D	*23*
B	*22*
ψ-AlCuFe[b]	21±0.5
ω-AlCuFe[b]	21
Al	*20.8*
C	*19*
I-AlCuFeB	18.1
	In water (Å)
QC-AlPdMn[a]	79–100±10
ψ-AlCuFe[b]	86±4.3
Alloy A	*78±6*
Al	*70.1*
AlCuFeCr	70±3.6
Alloy C	*69±1*
β-AlCuFe[b]	67±2.8
Alloy B	*61±4*
λ-AlCuFe[b]	58±3.6
Alloy D	*49±2*

[a] Refer Ref. [10].
[b] Refer Ref. [11].
[c] Refer Ref. [6].

which alloys with higher Cr content can more easily form the graded Al–Cr-oxide skin, and that this is a more effective barrier against further reaction than Al-oxide alone.

5. Conclusion

In summary, we have found that Cr appears to enhance the oxidation-resistance of a family of Al–Cr–Fe quasicrystalline approximants. Oxidation results in an outer layer which is primarily Al-oxide. Under severe conditions, Cr can also oxidize. We hypothesize that Cr-oxide may develop below the Al-oxide, forming a double barrier against further reaction. The third component, Fe, is protected in all cases.

Acknowledgements

We thank V. Fournée for useful discussions and for data from his own work. We gratefully acknowledge the financial support which enabled this collaboration. For the Ames group, this is from the National Science Foundation under Grant No. INT-9726785 and through the US Department of Energy under Contract No. W-405-Eng-82. For the Nancy group, this is from the CNRS, local authorities and PICS No. 545.

References

[1] J.M. Dubois, S.S. Kang, Y. Massiani, J. Non-Cryst. Sol. 153–154 (1993) 443.
[2] J.M. Dubois, S.S. Kang, A. Perrot, Mater. Sci. Eng. A 179–180 (1994) 122.
[3] J.M. Dubois, A. Proner, B. Ducaille, P. Cathonnet, C. Dong, V. Richardt, Y. Massiani, S. Ait-Yaazza, E. Belin-Ferré, Ann. Chim. Mater. 19 (1994) 3.
[4] S.S. Kang, J.M. Dubois, J. Von Stebut, J. Mater. Res. 8 (1993) 2471.
[5] N. Rivier, J. Non-Cryst. Sol. 153–154 (1993) 458.
[6] S.L. Chang, J.W. Anderegg, P.A. Thiel, J. Non-Cryst. Sol. 195 (1996) 95.
[7] C.J. Jenks, S.L. Chang, J.W. Anderegg, M.F. Besser, D.J. Sordelet, P.A. Thiel, in: A.I. Goldman, D.J. Sordelet, P.A. Thiel, J.M. Dubois (Eds.), New Horizons in Quasicrystals, World Scientific, Singapore, 1996, p. 157.
[8] C.J. Jenks, S.L. Chang, J.W. Anderegg, P.A. Thiel, D.W. Lynch, Phys. Rev. B 54 (1996) 9.
[9] C.J. Jenks, P.J. Pinhero, T.E. Bloomer, S.L. Chang, J.W. Anderegg, P.A. Thiel, in: S. Takeuchi, T. Fujiwara (Eds.), Proceedings of the Sixth International Conference on Quasicrystal, World Scientific, Singapore, 1997, p. 761.
[10] P.J. Pinhero, S.L. Chang, J.W. Anderegg, P.A. Thiel, Phil. Mag. B 75 (1997) 271.
[11] P.J. Pinhero, D.J. Sordelet, J.W. Anderegg, P. Brunet, J.M. Dubois, P.A. Thiel, Mater. Res. Soc. Symp. 583 (1999) 263.

[12] P.J. Pinhero, J.W. Anderegg, D.J. Sordelet, T.A. Lograsso, D.W. Delaney, P.A. Thiel, J. Mater. Res. 14 (1999) 8.
[13] P.J. Pinhero, J.W. Anderegg, D.J. Sordelet, M.F. Besser, P.A. Thiel, Phil. Mag. B 79 (1999) 91.
[14] H.E. Boyer, T.L. Gall (Eds.), Metals Handbook Desk Edition, American Society for Metals, Metal Park, OH, 1984.
[15] V. Demange, J.S. Wu, V. Brien, F. Machizaud, J.M. Dubois, Mater. Sci. Eng. 294–296 (2000) 79.
[16] H.X. Sui, X.Z. Liao, K.H. Kuo, Phil. Mag. Lett. 71 (1995) 139.
[17] H.X. Sui, X.Z. Liao, K.H. Kuo, X. Sou, S. Hovmöller, Acta Cryst. 1353 (1997) 587.
[18] A.J. Bradley, S.S. Lu, Z. Krist. 96 (1937) 20.
[19] S. Ebalard, F. Spaepen, J. Mater. Res. 6 (1991) 1641.
[20] H. Selke, U. Vogg, P.L. Ryder, Phil. Mag. B 65 (1992) 421.
[21] V. Khare, N.P. Lalla, R.S. Tiwari, O.N. Srivastawa, J. Mater. Res. 10 (1995) 1905.
[22] C. Dong, Phil. Mag. A 73 (1996) 1519.
[23] S.P. Ge, K.H. Kuo, J. Mater. Res. 14 (1999) 2799.
[24] C. Dong, J.M. Dubois, CNRS Research Report, Ecole des Mines de Nancy, 54042 Nancy Cedex, France, 1992, unpublished.
[25] X.Z. Li, C. Dong, J.M. Dubois, J. Appl. Cryst. 28 (1995) 96.
[26] J.F. Moulder, W.F. Stickle, P.E. Sobol, K.D. Bomben, Handbook of X-ray Photoelectron Spectroscopy, Perkin Elmer, Eden Prairie, MN, 1992.
[27] D. Briggs, M.P. Seah (Eds.), Practical Surface Analysis, Vol. 1, Auger and X-ray Photoelectron Spectroscopy.
[28] B.R. Strohmeier, Surf. Interf. Anal. 15 (1990) 51.
[29] S. Tanuma, C.J. Powell, D.R. Penn, Surf. Interf. Anal. 11 (1988) 577.
[30] R. Lide (Ed.), Handbook of Chemistry and Physics, 78th Edition, CRC Press, Boca Raton, FL, 1997.